analytical chemistry

pubs.acs.org/ac Article

Drug Screening for Glycolysis Pathway in Living Cancer Cells Using ^{19}F NMR

Biao Liu, Tao Huang, Xiong Xiao, Xin Chai, Yating Lei, Qiuyun Sun, Qin Hu, Qinjun Zhu, Danyun Zeng, Caixiang Liu, Lichun He, Zhou Gong, Bin Jiang, Xin Zhou, Maili Liu,* and Xu Zhang*

Cite This: *Anal. Chem.* 2025, 97, 9192−9201 Read Online

ACCESS | Metrics & More | Article Recommendations | Supporting Information

ABSTRACT: Glycolysis is a fundamental process for the generation of cellular energy, and its dysregulation has been linked to a number of diseases, including obesity, neurological disorders, and cancer. Targeting glycolysis is therefore a promising therapeutic strategy. However, effective drugs that specifically target glycolysis are still lacking. In this study, we introduce a novel approach utilizing ^{19}F NMR to monitor early glycolysis in living MCF-7 cells. By tracking metabolites downstream of the glucose analogue 2-fluoro-2-deoxyglucose (2-FDG), we successfully observed the activity of key glycolytic components, such as glucose transporters (GLUTs) and hexokinase (HKs). Our results reveal distinct metabolic profiles upon inhibition of these targets, advancing the understanding of glycolytic regulation. In addition, we applied this approach to screen traditional Chinese medicines for their effects on glycolysis and identified *Salvia miltiorrhiza* and *Fructus evodiae* as modulators with contrasting effects on glycolytic metabolism. This dual modulation highlights their potential as valuable tools for therapeutic intervention. Our study provides an innovative methodology for both the exploration of glycolytic pathways and the discovery of novel therapeutics, offering new perspectives for drug development targeting metabolic diseases.

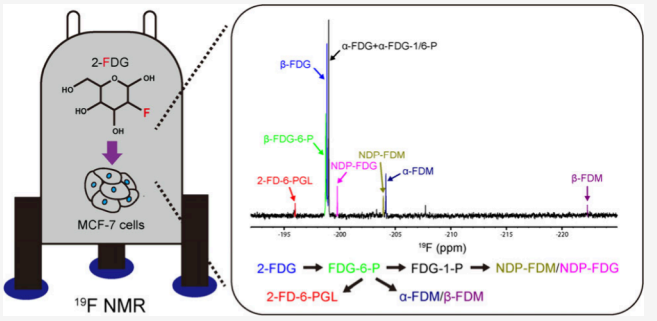

INTRODUCTION

Glucose is the primary nutrient source of energy and a crucial metabolic intermediate in living cells. Glycolysis, a core pathway of glucose metabolism, plays a pivotal role in energy metabolism and biosynthesis,[1] converting glucose into pyruvate with concurrent ATP generation.[2] Its dysregulation is closely linked to various diseases, including cancer,[3] neurological disorders,[4] and diabetes.[5] For example, cancer cells exhibit abnormal glycolysis, known as the "Warburg effect", which is characterized by increased glucose uptake to support rapid proliferation.[6] Consequently, glycolysis is a major focus for therapeutic targeting.[7]

Despite extensive research into glycolytic enzymes,[8] such as glucose transporters (GLUTs), hexokinases (HKs), phosphofructokinase (PFK), glyceraldehyde-3-phosphate dehydrogenase (GAPDH), phosphoglycerate mutase 1 (PGAM1), pyruvate kinase M2 (PKM2), lactate dehydrogenase A (LDHA), monocarboxylate transporters (MCTs) and pyruvate dehydrogenase kinase (PDK),[9] and the identification of numerous natural and synthetic molecules capable of modulating glycolysis.[10,11] However, glycolysis is indeed a fundamental metabolic pathway present in nearly all cells, which complicates the development of specific inhibitors. Many glycolysis inhibitors have been abandoned due to their low specificity and significant side effects, underscoring the need for innovative approaches to drug discovery.

Understanding the pathological process of disease and identifying therapeutic targets can be greatly enhanced by discovering and identifying small molecule metabolites and metabolic pathway alterations.[12] Recent advances in small-molecule-based metabolomics have revolutionized early stage drug development.[13−15] However, traditional metabolomics approaches, relying on metabolite extraction, fail to capture the dynamic nature of cellular metabolism.[16] This limitation has spurred the development of real-time, noninvasive methods for studying the metabolic flux in living cells.

Techniques such as glucose uptake and lactate excretion measurements,[17] ATR-FTIR spectroscopy,[18] and various assays provide valuable data, but they often lack the comprehensive view required to fully interpret the complex, multienzymatic process of glycolysis. Nuclear magnetic resonance (NMR) has emerged as a powerful tool for

Received: November 14, 2024
Revised: April 10, 2025
Accepted: April 22, 2025
Published: April 28, 2025

https://doi.org/10.1021/acs.analchem.4c06149
Anal. Chem. 2025, 97, 9192−9201

noninvasive, real-time investigation of cellular metabolism.[19] Recent innovations in bioreactor design have enabled long-term intracellular NMR studies,[20] allowing for detailed observation of metabolic processes and drug effects.[21−24]

To address the challenge of complex background signals in cellular, isotope-labeled probe molecular are commonly employed.[25] However, their use is often hindered by low sensitivity. In contrast, ^{19}F NMR presents a compelling alternative, offering high sensitivity and clear signal separation from the cellular background. ^{19}F has been widely used to study the interaction of proteins and ligands within living cells, and has great potential for the discovery of effective compounds in the early stages of drug development.[26−28]

2-Fluoro-2-deoxyglucose (2-FDG) is a fluorinated analogue of glucose. Although ^{18}F-FDG has been used as a PET tracer to assess glucose utilization in both normal and pathological tissues,[29−31] ^{19}F-FDG has also been used as an NMR probe to study metabolism in cells, tissues and organs. For example, ^{19}F-FDG has been used to investigate glucose metabolism in yeast cells[32] and to quantify the equilibrium exchange kinetics of carrier-mediated transmembrane transport of fluorinated substrates in cells.[33] In addition, it has been used as a tracer to evaluate tissue-specific glucose utilization in rats,[34] highlighting its versatility as a metabolic probe. These studies underscore the potential of ^{19}F-FDG as a tool for high-resolution metabolic profiling.

In this study, we introduced a novel ^{19}F NMR-based approach to monitor glycolysis in living cells using 2-FDG. This method enables real-time tracking of 2-FDG metabolism, providing unprecedented insight into glycolytic enzyme activity, and facilitating high-throughput screening of potential inhibitors. We validate this approach by monitoring 2-FDG metabolism in the presence of known glycolytic inhibitors, and extend its application to screen traditional Chinese medicines (TCMs). Notably, our screening identified *Salvia miltiorrhiza* and *Fructus evodiae* as significant modulators of cellular glycolytic metabolism, with opposite effects on ^{19}F NMR spectra. This finding not only demonstrates the utility of our method in natural product screening, but also opens new avenues for understanding the metabolic impacts of TCMs.

This study presents a significant advance in metabolic research methodology, offering a powerful tool for real-time glycolysis monitoring and drug discovery. By combining the sensitivity of ^{19}F NMR with the metabolic relevance of 2-FDG, we provide a platform that bridges the gap between *in vitro* enzyme assays and *in vivo* metabolic studies, potentially accelerating the development of novel therapeutics that target cellular metabolism.

EXPERIMENTAL SECTION

Chemicals and Materials. Reagents and solvents of commercial quality were used without additional purification, unless otherwise specified. 2-FDG was sourced from Sigma-Aldrich (Merck, Burlington, MA, USA). BAY-876 and 2-DG were obtained from MedChem Express (MCE, USA). The TCMs were purchased from the Chinese Medicinal Materials Wholesale Supermarket (Anhui, China).

Cell Culture. HepG2 and HeLa cells were obtained from the China Center for Type Culture Collection (Wuhan, China). The immortalized human HSC cell line LX2 was obtained from Procell (Wuhan, China), while MCF-7 cells were obtained from the National Collection of Authenticated Cell Cultures (Shanghai, China). All cells were cultured in Dulbecco-modified Eagle medium (DMEM) high glucose (Gibco, USA) supplemented with 100 U/mL penicillin, 100 μg/mL streptomycin and 10% fetal bovine serum (FBS, Gibco, USA). Cultures were maintained in uncoated 175 cm^2 plastic flasks and incubated at 37 °C with 5% CO_2 in a humidified atmosphere. Passage was performed every 2−3 days using 0.05% trypsin-EDTA. Cell numbers were determined using an automatic cell counter (BIO-RAD, USA). Cells were resuscitated 2 days prior to agarose thread production.

Production of Agarose Threads. The production method for agarose threads was as previously described.[35] Briefly, low-gelling agarose (Sigma-Aldrich, A4018) was dissolved at 1.5% (w/v) in H_2O at 85 °C, sterilized by filtration through a 0.22 μm filter, aliquoted in Eppendorf tubes, and stored at 4 °C. For sample preparation, one aliquot of solidified agarose was melted at 85 °C in a water bath and then maintained in solution at 37 °C in a thermoblock. Two pellets of MCF-7 cells collected from two 175 cm^2 flasks (approximately 1−2 × 10^7 cells) were heated at 37 °C for 15−20 s in the thermoblock. Cells were then resuspended in 300 μL of agarose solution, taking care to avoid bubble formation. The cell-agarose suspension was aspirated into a chromatography PEEK tubing (outer diameter 1/16″, inner diameter 0.75 mm) connected to a 1 mL syringe and cooled down at room temperature for 2 min. Agarose threads were cast into the NMR flow unit tube using a 10 mL syringe.

Bioreactor Setup. The NMR bioreactor was set up following a previously reported procedure.[35,36] A total of 20 mL of circulating medium consisting of 90% DMEM, 10% FBS, 1% antibiotics, and 10% D_2O was used to maintain cell growth in the NMR tube. The medium, placed in a 37 °C water bath, was continuously circulated for 10 h at a rate of 0.1 mL/min. A 0.22 μm filter was positioned at the end of the flow tube to avoid bacterial contamination of the circulating medium. An identical filter was added to the front end of the peristaltic pump to minimize the influence of bubbles in the NMR tube. At the end of each experiment, the bioreactor was rinsed with sterile water and acid−base solutions. The rinsing process involved flowing 0.2 M sodium hydroxide, 3 M citric acid and 0.2 M sodium hydroxide for 10 min each, followed by 30 min of water rinsing at the same flow rate.

Preparation of Cell Lysate. MCF-7, LX2, HepG2 and HeLa cells were revived and cultured in an incubator for 48 h. After incubation, the spent culture medium was aspirated, and the cells were washed once with PBS. Subsequently, DMEM medium containing 0.25 mM 2-FDG was added, and the cells were further incubated for 10 h. The cells in the culture flask were then trypsinized, and the resulting cell pellet was collected. The pellet was resuspended in 600 μL of PBS and lysed using an ultrasonic cell disrupter for 5 min. The lysate was centrifuged at 12,000 rpm for 5 min, and the supernatant was collected. The supernatant was mixed with 10% D_2O prior to ^{19}F NMR spectra acquisition.

Preparation of NMR Samples of MCF-7 Cells Treated with Traditional Chinese Medicine. MCF-7 cells were revived and cultured in an incubator for 48 h. The culture medium was then replaced with DMEM medium containing 0.25 mM 2-FDG. After 5 h of incubation, traditional Chinese medicine extracts dissolved in DMSO-d_6 were added to the medium. The cells were incubated for an additional 5 h, after which the MCF-7 cell pellet was collected and washed once with PBS. The cell pellet was resuspended in 300 μL of medium containing 10% D_2O and transferred to a Shigemi

https://doi.org/10.1021/acs.analchem.4c06149
Anal. Chem. 2025, 97, 9192−9201

NMR tube. The sample was centrifuged at 20 × *g* for 20 s using a custom centrifuge and then rapidly transferred to the magnet for NMR acquisition.

NMR Experiments and Data Processing. NMR spectra were collected at 310 K using a 600 MHz Bruker AVANCE spectrometer equipped with a cyroprobe. The ^{19}F NMR spectra consisted of 1300 scans with a relaxation delay of 1s. ^{19}F spectra were acquired with ^{1}H decoupling and processed using an exponential window function with 5 Hz line broadening. The ^{19}F NMR spectra were acquired with a spectral width of 40 ppm, centered at −210.0 ppm. The number of sampling points in the NMR experiment was 12K, and the acquisition time for each spectrum was 28 min and 14 s. ^{19}F chemical shifts were referenced to hexafluorobenzene at −161.945 ppm. Data processing and analysis were performed using Bruker Topspin 4.0.1 software (Bruker, Billerica, MA, USA).

LDH Activity Measurement. Lactate dehydrogenase (LDH) activity was measured using the LDH Release Assay Kit (catalog number C0016; Beyotime, China) following the manufacturer's instructions.

Crude Extraction of Traditional Chinese Medicine. All TCMs were soaked in 80−90% alcohol for 5 days before ultrasonication. The resulting mixture was filtered through a 0.22 μm membrane and subjected to rotary evaporation. After most of the liquid evaporated, the remaining material underwent vacuum drying to remove any residual solvent. The resulting herbal extract powder was weighed using an analytical balance and dissolved in DMSO. In the TCM screening experiment, the final concentration of all TCMs used was 0.8 mg/mL.

Cell Proliferation Assays. To determine the impact of TCMs on MCF-7 cell viability, cell proliferation was evaluated using the Super-Enhanced Cell Counting Kit-8 (catalog number C0048; Beyotime, China). The assay involved incubating cells with Super-Enhanced CCK-8 for 30 min, followed by absorbance measurement at 450 nm using a SpectraMax i3x plate reader.

Trypan Blue Assays. Trypan blue staining was used to access cell viability post-NMR experiments. After NMR experiments, cells were centrifuged at 200×*g* for 5 min. The cells were then resuspended with 10 mL PBS. The cell suspension was mixed with 0.4% trypan blue (catalog number ST2780; Beyotime, China) at a 1:1 ratio for 3 min. Subsequently, 10 μL of the stained mixture was transferred to a cell counting plate, and cell viability was determined using an automatic cell counter.

Statistical Analysis. All data are presented as mean ± standard deviation from three independent experiments except the TCMs screening experiment. Statistical analyses were performed using one-way ANOVA for comparison at final time points in real-time ^{19}F NMR experiments. Asterisks denote significance levels (*) for *P*-values < 0.05, and "ns" indicates no statistically significant difference.

RESULTS AND DISCUSSION

Characterization of Glycolytic Metabolic Features in Four Different Cell Lines. ^{13}C-glucose is a primary tracer for monitoring intracellular glycolytic metabolism. However, its use is often limited by background signals from cells and media, which can hinder the acquisition of high-resolution spectra in a short time frame. Although 2-FDG has a lower binding affinity for hexokinase compared to glucose and cannot be fully metabolized,[37] it accumulates intracellularly in proportion to the glycolytic rate of the cell.[38] This unique property of 2-FDG allows it to serve as a reliable probe for monitoring early glycolysis, despite its lower enzymatic affinity compared to glucose.

Upon cellular uptake, 2-FDG is metabolized into several key metabolites, including 2-fluoro-2-deoxy-D-mannose (2-FDM), 6-phospho-2-fluoro-2-deoxy-D-gluconolactone (2-FD-6-PGL), 2-fluoro-2-deoxy-D-glucose-6-phosphate (2-FDG-6-P), and 2-fluoro-2-deoxy-D-mannose-6-phosphate (FDM-6-P).[34,39,40] While ^{18}F 2-FDG PET is FDA-approved for measuring regional glucose uptake to aid in diagnosing seizures,[41] the use of ^{19}F 2-FDG detected by NMR allows for a more detailed analysis of its metabolism, encompassing not only its uptake but also its entire metabolic pathway. These metabolic processes involve key enzymes such as GLUTs and HKs (Figure 1a), making fluorinated metabolites sensitive indicators of enzyme activity.

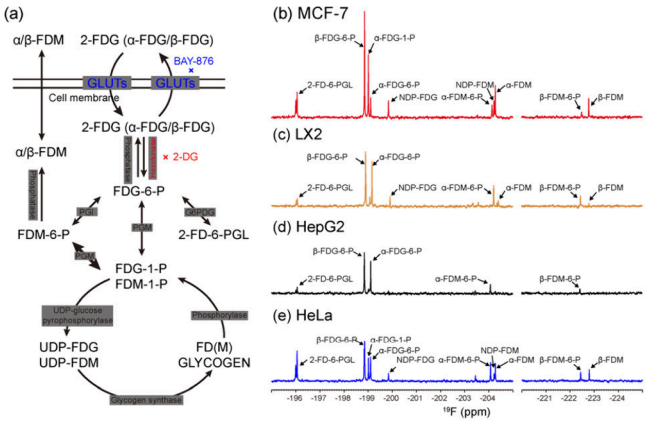

Figure 1. (a) Schematic illustration of potential metabolic pathways of 2-FDG in cells. 2-FDG: 2-fluoro-2-deoxy-D-glucose. GLUTs: glucose transporters. FDG-6-P: 2-fluoro-2-deoxy-D-glucose-6-phosphate. FDM-6-P: 2-fluoro-2-deoxy-D-mannose-6-phosphate. FDG-1-P: 2-fluoro-2-deoxy-D-glucose-1-phosphate. FDM-1-P: 2-fluoro-2-deoxy-D-mannose-1-phosphate. UDP: uridine diphosphate. PGM: phosphoglucomutase. PGI: phosphoglucose isomerase. 2-FD-6-PGL, 6-phospho-2-fluoro-2-deoxy-D-gluconolactone. G6PDH: glucose-6-phosphate dehydrogenase. ^{19}F spectra of cellular metabolites extracted from (b) MCF-7, (c) LX2, (d) HepG2, and (e) HeLa cells after treatment with 0.25 mM 2-FDG for 10 h. Metabolites were identified based on published chemical shift data.[34,44] See Table S1 for detailed assignments.

We investigated the metabolism of 2-FDG in four cell types and identified distinct signals in their NMR spectra (Figure 1b−e). FDG uptake by tumor cells is associated with elevated expression of glucose transporter molecules on the cell surface and increased levels of hexokinase within these cells.[38] Differences in enzyme expression levels among cell types can lead to variations in the relative metabolites content of 2-FDG, which may not fully reflect the overall glycolytic process of glucose. Notably, MCF-7 cells exhibited the highest levels of fluorinated metabolites, consistent with their high enzyme expression and glycolysis efficiency.[42] Given this metabolic dependency in cancer cells, targeting glycolysis holds therapeutic potential.[43]

While 2-FDG provides a useful alternative for assessing glycolytic activity, it is important to recognize that its metabolic fate differs from that of glucose, which could lead

https://doi.org/10.1021/acs.analchem.4c06149
Anal. Chem. 2025, 97, 9192−9201

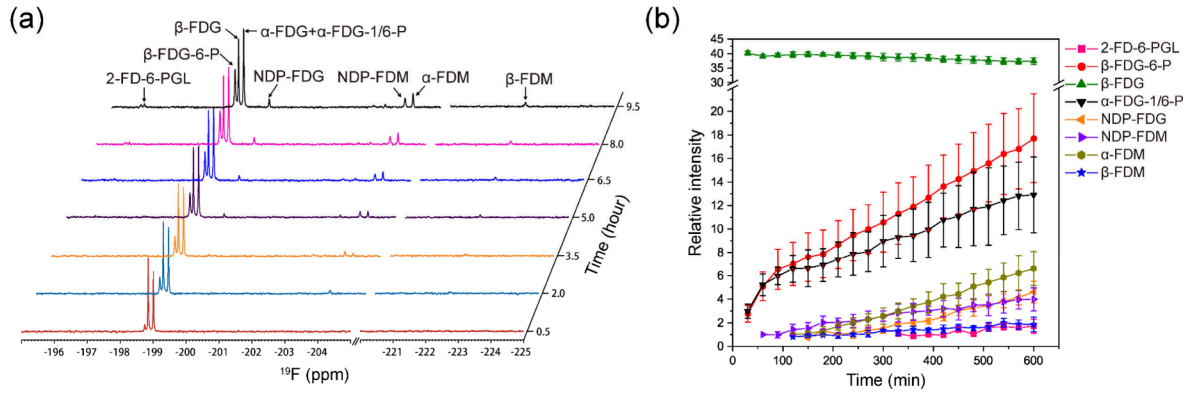

Figure 2. (a) ^{19}F spectra showing the metabolism of 2-FDG in MCF-7 cells at 0.5, 2.0, 3.5, 5.0, 6.5, 8.0, and 9.5 h. (b) Time-dependent metabolic changes in MCF-7 cells treated with 0.25 mM 2-FDG; each group had three replicates.

Table 1. Relative Rate of 2-FDG Metabolites, Fitted Data from 330 min to 600 min

2-FDG metabolites	2-FD-6-PGL	*β*-FDG-6-P	*β*-FDG	*α*-FDG-1/6-P	NDP-FDG	NDP-FDM	*α*-FDM	*β*-FDM
Relative rate ($\times 10^{-4}$ min^{-1})	27.7 ± 11.4	238.1 ± 4.4	−57.7 ± 5.2	148.1 ± 6.8	89.2 ± 7.3	46.7 ± 2.6	134.1 ± 2.9	24.4 ± 4.1

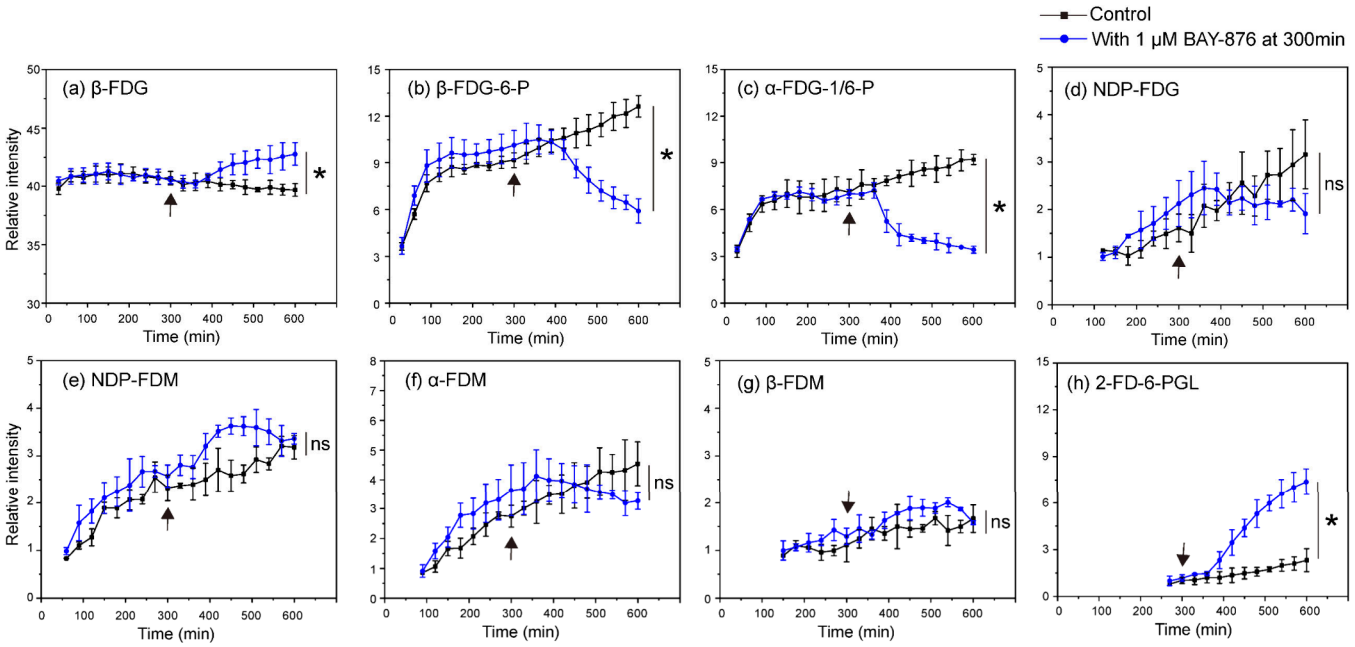

Figure 3. Time-dependent metabolic changes in MCF-7 cells treated with (blue line) or without (black line) 1 μM BAY-876 for 300 min. Each group had three replicates. (a) *β*-FDG; (b) *β*-FDG-6-P; (c) *α*-FDG-1/6-P; (d) NDP-FDG; (e) NDP-FDM; (f) *α*-FDM; (g) *β*-FDM; (h) 2-FD-6-PGL. Statistical significance was assessed by one-way ANOVA. ns: not significant. *: *P*-value < 0.05. Arrows indicate the time at which BAY-876 was added to the medium.

to variations in observed enzymatic activity and metabolite distribution. Our comprehensive mapping of 2-FDG metabolism in MCF-7 cells positions them favorably for screening novel therapies targeting these pathways.

Real-Time Characterization of Glycolysis Using 2-FDG. In order to map 2-FDG metabolism in MCF-7 cells in real time, we used a bioreactor to maintain cell activity within the NMR tube over an extended period of time. Despite the signal broadening in the NMR spectra due to the intracellular environment, we still identified several critical metabolites. As 2-FDG metabolizes, its downstream metabolites gradually accumulate (Figure 2a).

The first detectable signal on the ^{19}F spectra is *β*-FDG-6-P, the initial product of 2-FDG metabolism. Subsequently, metabolites such as NDP-FDG, *α*-FDM, and 2-FD-6-PGL appear sequentially, corresponding to different steps in the glycolytic pathway involving altered key enzymes such as GLUTs and HKs (Figure 1a). This allows us to directly observe activity of glycolysis in living cells.

Given that real-time metabolic changes are direct reflections of enzyme activity, this method enables the quantification of enzyme activity. To further validate this capability, we quantified the signal intensities of these metabolites over time to access the activity of the enzymes involved in different steps of the glycolytic pathway (Figure 2b).

In the living cell system, signal broadening caused by the crowded intracellular environment, resulted in the overlap of resonances between *α*-FDG and *α*-FDG-1/6-P (Figure 2a). To

https://doi.org/10.1021/acs.analchem.4c06149
Anal. Chem. 2025, 97, 9192−9201

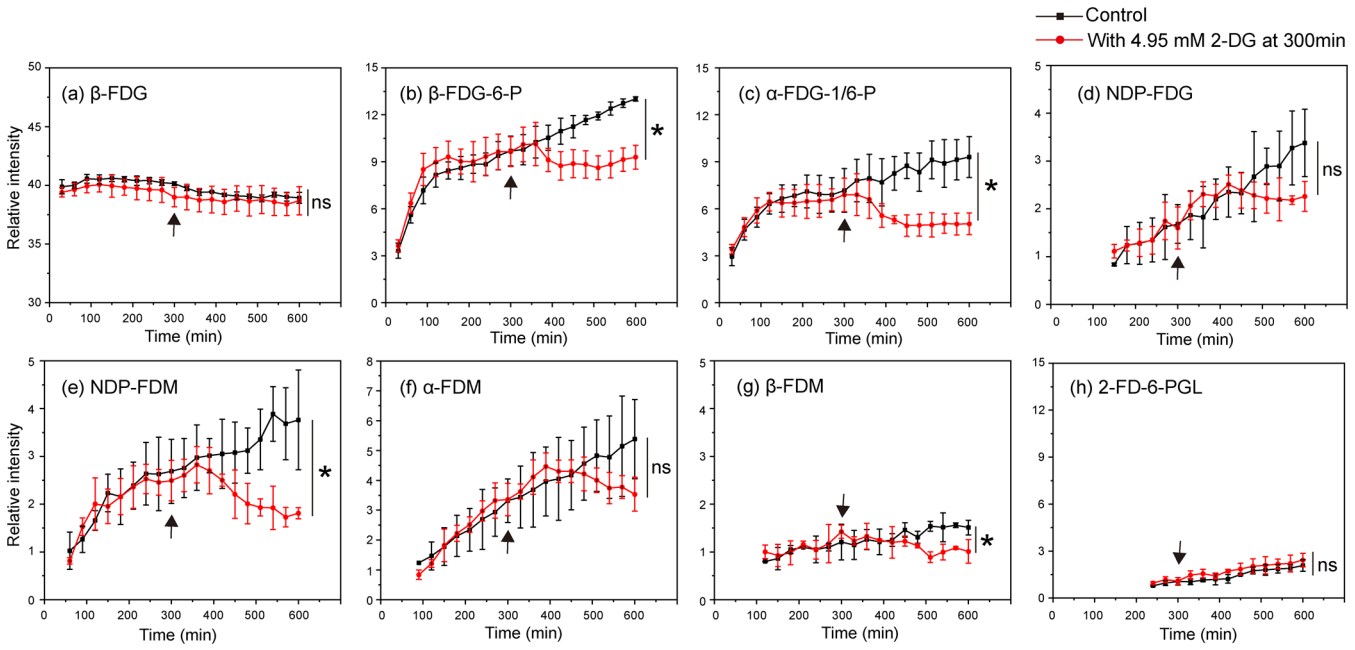

Figure 4. Time-dependent metabolic changes in MCF-7 cells treated with (red line) or without (black line) 4.95 mM 2-DG for 300 min. Each group had three replicates. (a) β-FDG; (b) β-FDG-6-P; (c) α-FDG-1/6-P; (d) NDP-FDG; (e) NDP-FDM; (f) α-FDM; (g) β-FDM; (h) 2-FD-6-PGL. Statistical significance was assessed by one-way ANOVA. ns: not significant. *: P-value < 0.05. Arrows indicate the time at which 2-DG was added to the medium.

address this, we calculated the relative intensities of these metabolites based on the known ratio of α-FDG to β-FDG (approximately 42:58).[45] The relative intensity of α-FDG-1/6-P was determined by subtracting the calculated intensity of α-FDG from the combined intensity of α-FDG and α-FDG-1/6-P. This approach allowed us to analyze the time-dependent changes in α-FDG-1/6-P accurately.

As 2-FDG is consumed, the concentrations of downstream products gradually increase, with their appearance following the sequence of 2-FDG metabolism. Notably, the production rate of β-FDG-6-P is significantly higher compared to the other metabolites, indicating this step occurs more rapidly (Table 1). This aligns with well documented overexpression of GLUTs in MCF-7 cells.

The absence of catabolites in the supernatant after the experiment (Figure S1) confirmed that the metabolism occurred within the MCF-7 cells, indicating the suitability of the approach for studying glycolysis in living systems.

Quantification of Glycolytic Inhibitor Effectiveness. Our real-time characterization method provides novel insights into the metabolic pathways of cancer cells, thereby opening up potential avenues for therapeutic interventions targeting glycolysis. The observed metabolic dynamics could serve as sensitive indicators of perturbations caused by therapeutic agents, making MCF-7 cells an ideal model for screening glycolysis-targeted treatments.

To further evaluate the ability of this method to characterize glycolytic enzymes as indicators of perturbations caused by therapeutic agents, we selected two inhibitors targeting different glycolytic enzymes: BAY-876, which acts on GLUTs, and 2-DG (2-deoxy-D-glucose), which acts on HKs (Figure 1a). Both inhibitors effectively block the glycolytic process.

BAY-876 is an inhibitor of GLUTs, which prevents glucose transport into the cell.[46] Although it contains fluorine, its signal does not overlap with these 2-FDG metabolites in the ^{19}F NMR spectrum (Figure S2). The addition of 1 μM BAY-876 at the 300 min mark (black arrows) inhibited β-FDG transport and halted its metabolism. However, the phosphorylation products β-FDG-6-P and α-FDG-1/6-P continued to be metabolized, resulting in a reduction of these phosphorylated products over time (Figure 3). Interestingly, downstream metabolites such as 2-FD-6-PGL increased over time, likely due to influence of the inhibitor. This highlights the ability to characterize the impact of GLUTs inhibition on glycolysis through changes in downstream metabolites.

2-DG is a glucose analogue and HK inhibitor that prevents glucose phosphorylation.[47] After 2-DG treatment, the metabolism of 2-FDG in MCF-7 cells initially remained unchanged, as it did not affect 2-FDG transport (Figure 4). However, it significantly reduced the levels of phosphorylation products such as β-FDG-6-P and α-FDG-1/6-P, as well as other downstream products, while, leaving 2-FD-6-PGL unaffected. This distinct metabolic signature of 2-FDG provides a clear contrast to the effects of BAY-876.

The level of lactate dehydrogenase (LDH) in the circulating medium did not increase significantly after the experiment, indicating that the cells remained viable (Figure S3). These findings demonstrate the robustness of our real-time NMR-based method for evaluating the efficacy of glycolytic inhibitors in living cells.

In comparison, measurements of glucose uptake and lactate excretion can evaluate overall glycolytic capacity but cannot reveal differences in the targets of action of specific inhibitors. Our method, which monitors and quantifies dynamic changes in metabolites in response to inhibitors, offers a powerful tool for developing and optimizing glycolysis-targeted cancer therapies.

Screening of Traditional Chinese Medicine for Glycolysis Modulation. Our approach was used to screen

https://doi.org/10.1021/acs.analchem.4c06149
Anal. Chem. 2025, 97, 9192−9201

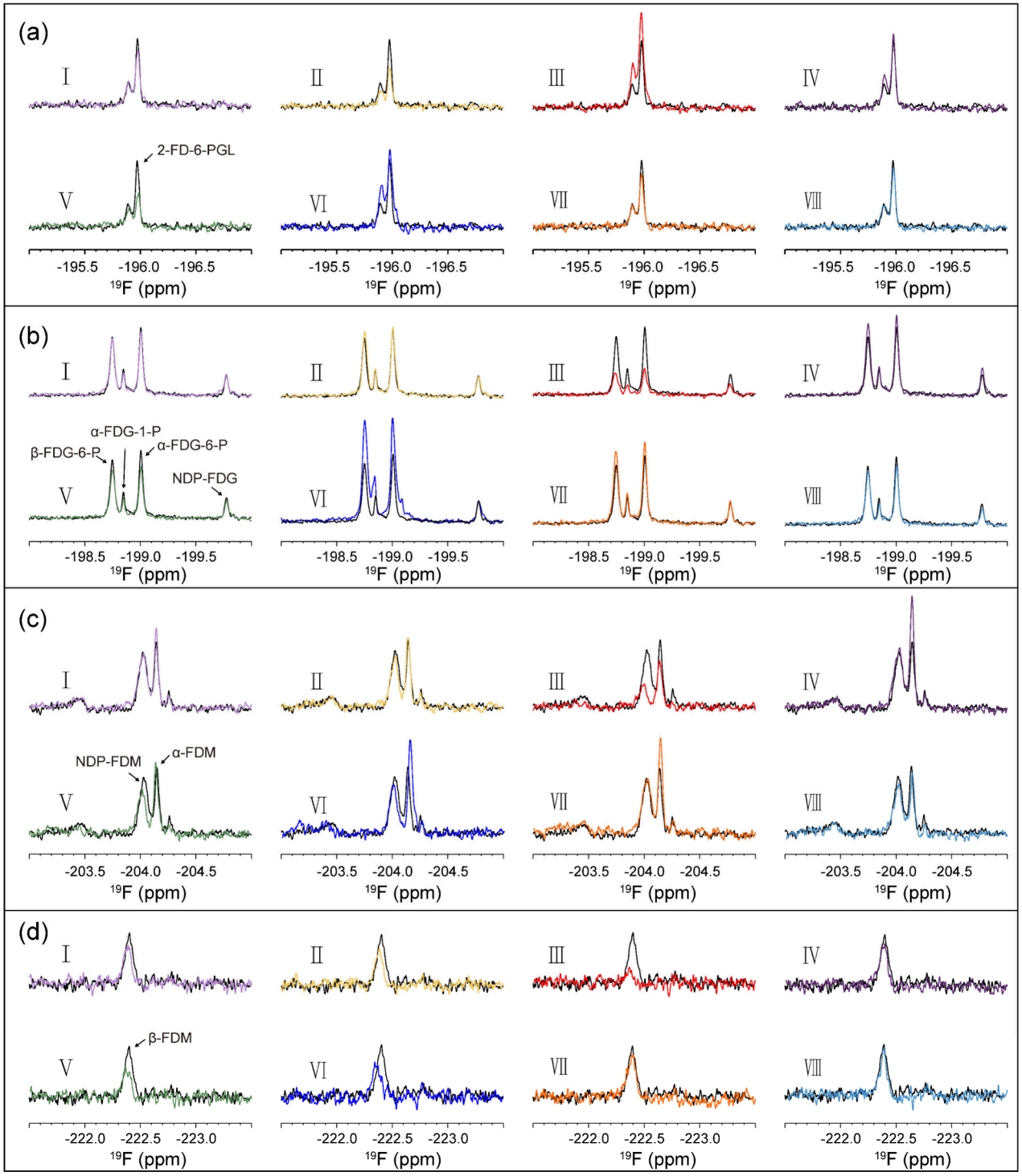

Figure 5. Overlays of ^{19}F-NMR spectra of the MCF-7 cells treated with control solution (black) and extracts from TCMs. Different chemical shift regions of the ^{19}F spectra, (a) −195.0 to −197.0 ppm, (b) −198.0 to −200.0 ppm, (c) −203.0 to −205.0 ppm, (d) −221.0 to −224.0 ppm. (I) *Polugonatum sibiricum*, (II) *Ligustrum lucidum* Ait., (III) *Salvia miltiorrhiza*, (IV) *Ophiopogon japonicus*, (V) Paeoniae radix rubra, (VI) *Fructus evodiae*, (VII) *Rhizoma atractylodis macrocephalae*, and (VIII) *Carthamus tinctorius* L.

TCMs for potential glycolytic inhibitory effects. Several TCMs were tested, including *Polygonatum sibiricum* (PS, Huangjing), *Ligustrum lucidum* Ait. (LLA, Nvzhenzi), *Salvia miltiorrhiza* (SM, Danshen), *Ophiopogon Japonicus* (OJ, Maidong), Paeoniae radix rubra (PRR, Chishao), *Fructus evodiae* (FE, Wuzhuyu), *Rhizoma atractylodis macrocephalae* (RAM, Baizhu), and *Carthamus tinctorius* L. (CTL, Honghua). At a concentration of 0.8 mg/mL, none of these TCMs showed significant cytotoxicity in MCF-7 cells (Figure S4).

Given the time-consuming nature of real-time NMR, we collect cells at specific time points after TCM treatment to improve efficiency and potential for high-throughput screening. Previous experiments have verified that significant differences can be detected after 1−5 h of inhibitor incubation. Therefore, all screening experiments were performed on MCF-7 cells,

https://doi.org/10.1021/acs.analchem.4c06149
Anal. Chem. 2025, 97, 9192−9201

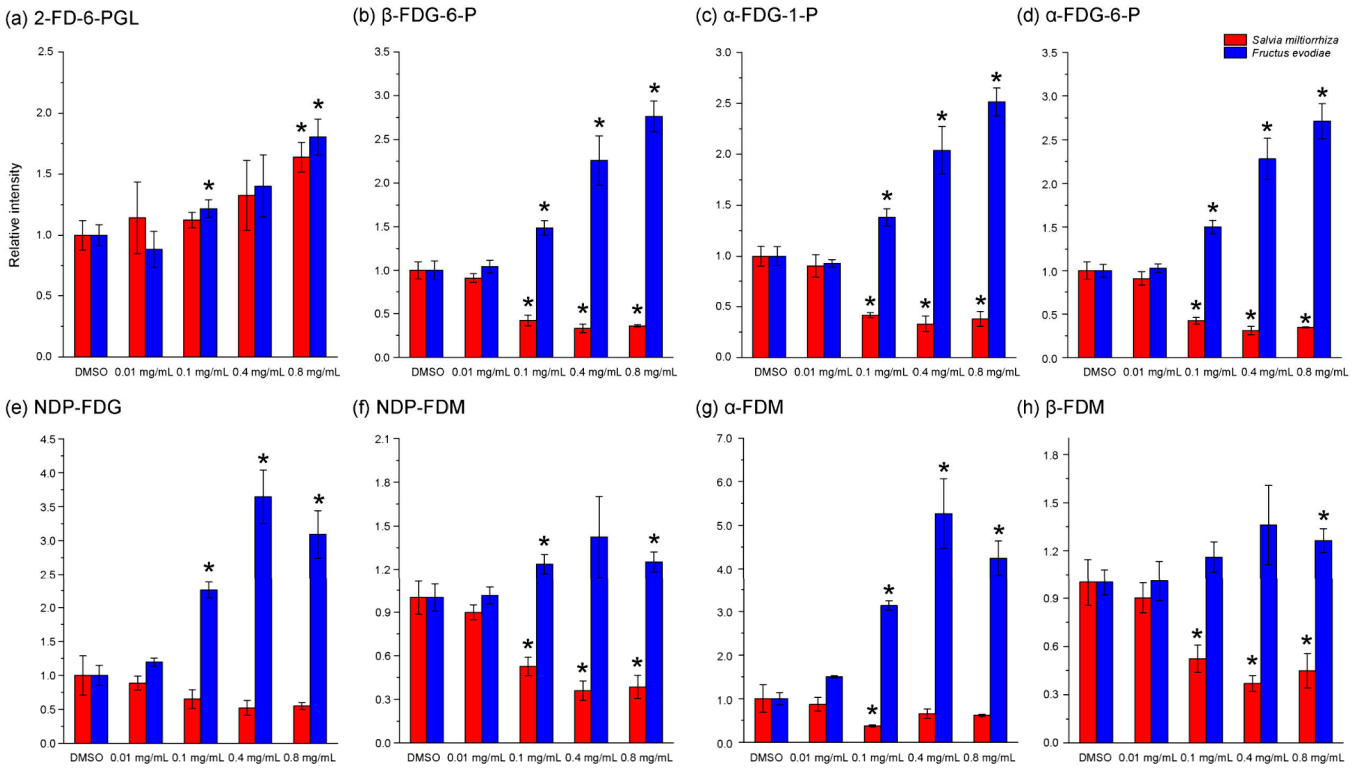

Figure 6. Changes in fluoride containing metabolites in MCF-7 cells treated with different concentrations of *Salvia miltiorrhiza* (red) and *Fructus evodiae* (blue). Each group had three replicates. (a) 2-FD-6-PGL; (b) *β*-FDG-6-P; (c) *α*-FDG-1-P; (d) *α*-FDG-6-P; (e) NDP-FDG; (f) NDP-FDM; (g) *α*-FDM; (h) *β*-FDM. Statistical significance was assessed by one-way ANOVA between different concentrations of TCMs and control. *: *P*-value < 0.05.

which were incubated with 0.25 mM 2-FDG for 5 h and then treated with TCM extracts for an additional 5 h. After this treatment, ^{19}F NMR spectra were collected from intact MCF-7 cells. Post-NMR cell viability experiments were confirmed using trypan blue staining (Figure S5).

Among the tested TCMs, only *Fructus evodiae* and *Salvia miltiorrhiza* significantly affected 2-FDG metabolism. *Fructus evodiae* promoted the production of fluorinated metabolites, while *Salvia miltiorrhiza* inhibited their production, except for 2-FD-6-PGL (Figure 5). Nevertheless, both TCMs show exhibited dose-dependent effects, indicating that they are effective in glycolysis (Figure 6). These opposite effects underline their potential as glycolytic modulators.

Fructus evodiae is known for its pharmacological effects, including analgesic,[48] anti-inflammatory,[49] antinociceptive[50] and antitumor effects,[51] but also exhibits cardiotoxicity[52] and hepatorenal toxicity, the pharmacological and toxicological mechanisms of which are not fully elucidated. Notably, in the presence of *Fructus evodiae*, we observed a significant increase in the production of 2-FD-6-PGL, *β*-FDG-6-P, *α*-FDG-6-P, *α*-FDG-1-P, NDP-FDG, and *α*-FDM. The increase in these fluorinated metabolites was dose-dependent (Figure 6), suggesting that *Fructus evodiae* can significantly enhance glucose metabolism. Given that liver diseases are often associated with abnormal glucose metabolism, our findings suggest that its stimulatory effect on glycolysis may contribute to its hepatorenal toxicity, although further research is needed to fully elucidate the underlying mechanisms.

Salvia miltiorrhiza has demonstrated broad antitumor activity,[53] in part through its active component Tanshinone IIA (Tan IIA), which inhibits glycolysis and the Warburg effect in cancer cells.[54,55] In the presence of *Salvia miltiorrhiza* extracts, MCF-7 cells showed a significant decrease in the production of *β*-FDG-6-P, *α*-FDG-6-P, *α*-FDG-1-P, NDP-FDG, NDP-FDM, *α*-FDM, and *β*-FDM, as the concentration of *Salvia miltiorrhiza* increased, the relative concentration of these metabolites decreased even more, indicating *Salvia miltiorrhiza* indeed inhibit the metabolism of glycolysis. However, there was a notable increase in the production of 2-FD-6-PGL, similar to the effects observed with the inhibitor BAY-876, suggesting that this TCM may have an effect on GLUTs in the cell line. Our ^{19}F NMR data are consistent with these findings and support the potential of *Salvia miltiorrhiza* as a glycolysis inhibitor.

These findings are highly significant as they demonstrate that our approach offers a robust tool for studying glycolysis and screening potential therapeutic agents. This method not only offers a platform for understanding the pharmacological actions of these TCMs, but also for identifying novel therapeutic strategies. Future studies can build on this foundation to explore the broader implications of glycolytic modulation by these and other TCMs, potentially leading to novel insights into cancer metabolism and treatment strategies.

Finally, several limitations of this study need to be acknowledged. First, real-time NMR experiments to capture dynamic changes of metabolites require considerable time, which is why we selected a specific time point for metabolite detection in our traditional Chinese medicine screening experiments. While this approach improves the efficiency of screening, it prevents us from obtaining dynamic information on how TCMs affect metabolites over time. Second, while 2-FDG and glucose share similar uptake and phosphorylation

https://doi.org/10.1021/acs.analchem.4c06149
Anal. Chem. 2025, 97, 9192−9201

mechanisms via GLUTs and HKs, their metabolic fates diverge due to the structural differences of 2-FDG. Specifically, 2-FDG cannot be fully metabolized like glucose, limiting its ability to reflect downstream metabolic processes. Nevertheless, 2-FDG accumulation within cells is proportional to glycolytic rate,[56] making it a reliable proxy for evaluating early glycolysis and glucose utilization.

In summary, we have proposed a novel method using 2-FDG as a probe to study glycolysis in living cells. This method has successfully enabled the screening of traditional Chinese medicine that influence cellular glycolytic metabolism.

CONCLUSION

Glycolysis is an important pathway for cellular energy production, and targeting this pathway is considered an effective strategy for treating various metabolic diseases, including cancer. However, the development of drugs that target glycolysis with high specificity and minimal side effects remains an ongoing challenge.

In this study, we have developed an innovative method for real-time monitoring of cellular glycolytic activity using ^{19}F NMR. By employing 2-FDG as a probe, this technique tracks downstream metabolic changes via ^{19}F NMR, providing a detailed assessment of the impact of key glycolytic enzymes. This approach allows the direct evaluation of the specific effects of GLUTs and HKs inhibitors on glycolysis. In addition, the static distribution of 2-FDG metabolites in MCF-7 cells was used to screen TCMs for their influence on glycolytic pathways. Our results suggest that *Salvia miltiorrhiza* and *Fructus evodiae* exert distinct modulatory effects on glycolytic metabolism. These results not only demonstrate the robust capacity of our method for exploring glycolytic processes in living cells, but also suggest a potential application of TCMs in the modulation of metabolic pathways.

Overall, our method provides a powerful tool for investigating glycolytic activity and screening potential therapeutic agents. Future research can build on these results to further explore the broader implications of glycolytic modulation by these and other TCMs, potentially leading to new insights and treatment strategies for metabolic diseases and cancer.

ASSOCIATED CONTENT

Supporting Information

The Supporting Information is available free of charge at https://pubs.acs.org/doi/10.1021/acs.analchem.4c06149.

Cell viability results, including CCK-8 assay, LDH activity measurement, and trypan blue staining; chemical shifts of 2-FDG metabolites from ^{19}F spectra (Table S1) (PDF)

AUTHOR INFORMATION

Corresponding Authors

Maili Liu − *Wuhan National Laboratory for Optoelectronics, Huazhong University of Science and Technology, State Key Laboratory of Magnetic Resonance Spectroscopy and Imaging, National Center for Magnetic Resonance in Wuhan, Wuhan Institute of Physics and Mathematics, Innovation Academy for Precision Measurement of Science and Technology, Chinese Academy of Sciences, Wuhan 430071, China; University of Chinese Academy of Sciences, Beijing 100049, China; Optics Valley Laboratory, Wuhan 430074, China;* orcid.org/0000-0002-9359-915X; Email: ml.liu@apm.ac.cn

Xu Zhang − *Wuhan National Laboratory for Optoelectronics, Huazhong University of Science and Technology, State Key Laboratory of Magnetic Resonance Spectroscopy and Imaging, National Center for Magnetic Resonance in Wuhan, Wuhan Institute of Physics and Mathematics, Innovation Academy for Precision Measurement of Science and Technology, Chinese Academy of Sciences, Wuhan 430071, China; University of Chinese Academy of Sciences, Beijing 100049, China; Optics Valley Laboratory, Wuhan 430074, China;* orcid.org/0000-0003-2481-946X; Email: zhangxu@apm.ac.cn

Authors

Biao Liu − *Wuhan National Laboratory for Optoelectronics, Huazhong University of Science and Technology, State Key Laboratory of Magnetic Resonance Spectroscopy and Imaging, National Center for Magnetic Resonance in Wuhan, Wuhan Institute of Physics and Mathematics, Innovation Academy for Precision Measurement of Science and Technology, Chinese Academy of Sciences, Wuhan 430071, China*

Tao Huang − *Wuhan National Laboratory for Optoelectronics, Huazhong University of Science and Technology, State Key Laboratory of Magnetic Resonance Spectroscopy and Imaging, National Center for Magnetic Resonance in Wuhan, Wuhan Institute of Physics and Mathematics, Innovation Academy for Precision Measurement of Science and Technology, Chinese Academy of Sciences, Wuhan 430071, China*

Xiong Xiao − *Wuhan National Laboratory for Optoelectronics, Huazhong University of Science and Technology, State Key Laboratory of Magnetic Resonance Spectroscopy and Imaging, National Center for Magnetic Resonance in Wuhan, Wuhan Institute of Physics and Mathematics, Innovation Academy for Precision Measurement of Science and Technology, Chinese Academy of Sciences, Wuhan 430071, China; University of Chinese Academy of Sciences, Beijing 100049, China*

Xin Chai − *Wuhan National Laboratory for Optoelectronics, Huazhong University of Science and Technology, State Key Laboratory of Magnetic Resonance Spectroscopy and Imaging, National Center for Magnetic Resonance in Wuhan, Wuhan Institute of Physics and Mathematics, Innovation Academy for Precision Measurement of Science and Technology, Chinese Academy of Sciences, Wuhan 430071, China*

Yating Lei − *Wuhan National Laboratory for Optoelectronics, Huazhong University of Science and Technology, State Key Laboratory of Magnetic Resonance Spectroscopy and Imaging, National Center for Magnetic Resonance in Wuhan, Wuhan Institute of Physics and Mathematics, Innovation Academy for Precision Measurement of Science and Technology, Chinese Academy of Sciences, Wuhan 430071, China; University of Chinese Academy of Sciences, Beijing 100049, China*

Qiuyun Sun − *Wuhan National Laboratory for Optoelectronics, Huazhong University of Science and Technology, State Key Laboratory of Magnetic Resonance Spectroscopy and Imaging, National Center for Magnetic Resonance in Wuhan, Wuhan Institute of Physics and Mathematics, Innovation Academy for Precision*

https://doi.org/10.1021/acs.analchem.4c06149
Anal. Chem. 2025, 97, 9192−9201

Measurement of Science and Technology, Chinese Academy of Sciences, Wuhan 430071, China

Qin Hu − *Wuhan National Laboratory for Optoelectronics, Huazhong University of Science and Technology, State Key Laboratory of Magnetic Resonance Spectroscopy and Imaging, National Center for Magnetic Resonance in Wuhan, Wuhan Institute of Physics and Mathematics, Innovation Academy for Precision Measurement of Science and Technology, Chinese Academy of Sciences, Wuhan 430071, China; University of Chinese Academy of Sciences, Beijing 100049, China*

Qinjun Zhu − *Wuhan National Laboratory for Optoelectronics, Huazhong University of Science and Technology, State Key Laboratory of Magnetic Resonance Spectroscopy and Imaging, National Center for Magnetic Resonance in Wuhan, Wuhan Institute of Physics and Mathematics, Innovation Academy for Precision Measurement of Science and Technology, Chinese Academy of Sciences, Wuhan 430071, China*

Danyun Zeng − *Wuhan National Laboratory for Optoelectronics, Huazhong University of Science and Technology, State Key Laboratory of Magnetic Resonance Spectroscopy and Imaging, National Center for Magnetic Resonance in Wuhan, Wuhan Institute of Physics and Mathematics, Innovation Academy for Precision Measurement of Science and Technology, Chinese Academy of Sciences, Wuhan 430071, China; University of Chinese Academy of Sciences, Beijing 100049, China*

Caixiang Liu − *Wuhan National Laboratory for Optoelectronics, Huazhong University of Science and Technology, State Key Laboratory of Magnetic Resonance Spectroscopy and Imaging, National Center for Magnetic Resonance in Wuhan, Wuhan Institute of Physics and Mathematics, Innovation Academy for Precision Measurement of Science and Technology, Chinese Academy of Sciences, Wuhan 430071, China; University of Chinese Academy of Sciences, Beijing 100049, China*

Lichun He − *Wuhan National Laboratory for Optoelectronics, Huazhong University of Science and Technology, State Key Laboratory of Magnetic Resonance Spectroscopy and Imaging, National Center for Magnetic Resonance in Wuhan, Wuhan Institute of Physics and Mathematics, Innovation Academy for Precision Measurement of Science and Technology, Chinese Academy of Sciences, Wuhan 430071, China; University of Chinese Academy of Sciences, Beijing 100049, China*

Zhou Gong − *Wuhan National Laboratory for Optoelectronics, Huazhong University of Science and Technology, State Key Laboratory of Magnetic Resonance Spectroscopy and Imaging, National Center for Magnetic Resonance in Wuhan, Wuhan Institute of Physics and Mathematics, Innovation Academy for Precision Measurement of Science and Technology, Chinese Academy of Sciences, Wuhan 430071, China; University of Chinese Academy of Sciences, Beijing 100049, China;* orcid.org/0000-0001-6883-4026

Bin Jiang − *Wuhan National Laboratory for Optoelectronics, Huazhong University of Science and Technology, State Key Laboratory of Magnetic Resonance Spectroscopy and Imaging, National Center for Magnetic Resonance in Wuhan, Wuhan Institute of Physics and Mathematics, Innovation Academy for Precision Measurement of Science and Technology, Chinese Academy of Sciences, Wuhan 430071, China; University of Chinese Academy of Sciences, Beijing 100049, China; Optics Valley Laboratory, Wuhan 430074, China;* orcid.org/0000-0002-1450-2269

Xin Zhou − *Wuhan National Laboratory for Optoelectronics, Huazhong University of Science and Technology, State Key Laboratory of Magnetic Resonance Spectroscopy and Imaging, National Center for Magnetic Resonance in Wuhan, Wuhan Institute of Physics and Mathematics, Innovation Academy for Precision Measurement of Science and Technology, Chinese Academy of Sciences, Wuhan 430071, China; University of Chinese Academy of Sciences, Beijing 100049, China; Optics Valley Laboratory, Wuhan 430074, China;* orcid.org/0000-0002-5580-7907

Complete contact information is available at: https://pubs.acs.org/10.1021/acs.analchem.4c06149

Author Contributions

The manuscript was written through contributions of all authors. All authors have given approval to the final version of the manuscript.

Notes

The authors declare no competing financial interest.

■ ACKNOWLEDGMENTS

This work was supported by National Key R&D Program of China (Grant 2023YFA1607500), Strategic Priority Research Program of the Chinese Academy of Sciences (Grant XDB0540000), National Natural Science Foundation of China (Grants 22174152, 22327901, 21505153, 21475146, 21991081, 21735007, and 32071990), and Hubei Provincial Natural Science Foundation of China (Grant 2023AFA041).

■ REFERENCES

(1) Zhang, Y.; Sampathkumar, A.; Kerber, S. M.-L.; Swart, C.; Hille, C.; Seerangan, K.; Graf, A.; Sweetlove, L.; Fernie, A. R. *Nat. Commun.* **2020**, *11* (1), 4509.

(2) DeBerardinis, R. J.; Lum, J. J.; Hatzivassiliou, G.; Thompson, C. B. *Cell Metab.* **2008**, *7* (1), 11−20.

(3) Yu, L.; Chen, X.; Sun, X. Q.; Wang, L. T.; Chen, S. W. *J. Cancer* **2017**, *8* (17), 3430−3440.

(4) Bell, S. M.; Burgess, T.; Lee, J.; Blackburn, D. J.; Allen, S. P.; Mortiboys, H. *Int. J. Mol. Sci.* **2020**, *21* (23), 8924.

(5) Guo, X.; Li, H.; Xu, H.; Woo, S.; Dong, H.; Lu, F.; Lange, A. J.; Wu, C. *Acta Pharm. Sinica B* **2012**, *2* (4), 358−367.

(6) Kim, J. W.; Dang, C. V. *Cancer Res.* **2006**, *66* (18), 8927−8930.

(7) Wang, Z.; Wang, N.; Chen, J.; Shen, J. *Evidence-Based Complementary Altern. Med.* **2012**, *2012*, No. 873175.

(8) Sheng, H.; Niu, B.; Sun, H. *Curr. Med. Chem.* **2009**, *16* (13), 1561−1587.

(9) Sheng, H. M.; Tang, W. J. *Recent Pat. Anti-Cancer Drug Discovery* **2016**, *11* (3), 297−308.

(10) Zhao, Y.; Chard Dunmall, L. S.; Cheng, Z.; Wang, Y.; Si, L. *Front. Pharmacol.* **2022**, *13*, No. 1036502.

(11) Chelakkot, C.; Chelakkot, V. S.; Shin, Y.; Song, K. *Int. J. Mol. Sci.* **2023**, *24* (3), 2606.

(12) Qiu, S.; Cai, Y.; Yao, H.; Lin, C.; Xie, Y.; Tang, S.; Zhang, A. *Signal Transduction Targeted Ther.* **2023**, *8* (1), 132.

(13) Kumar, A.; Misra, B. B. *Proteomics* **2019**, *19* (21−22), No. e1900042.

(14) Alarcon-Barrera, J. C.; Kostidis, S.; Ondo-Mendez, A.; Giera, M. *Drug Discovery Today* **2022**, *27* (6), 1763−1773.

(15) Tiziani, S.; Kang, Y. Y.; Choi, J. S.; Roberts, W.; Paternostro, G. *Nat. Commun.* **2011**, *2*, 545.

(16) Monteiro, M. S.; Carvalho, M.; Bastos, M. L.; Guedes de Pinho, P. *Curr. Med. Chem.* **2013**, *20* (2), 257−271.

(17) TeSlaa, T.; Teitell, M. A. *Methods Enzymol.* **2014**, *542*, 91−114.
(18) Poonprasartporn, A.; Chan, K. L. A. *Biochim Biophys Acta Mol. Cell Res.* **2021**, *1868* (7), No. 119024.
(19) Luchinat, E.; Banci, L. *Rend. Fis. Acc. Lincei* **2023**, *34* (3), 653−661.
(20) Luchinat, E.; Barbieri, L.; Campbell, T. F.; Banci, L. *Anal. Chem.* **2020**, *92* (14), 9997−10006.
(21) Alshamleh, I.; Krause, N.; Richter, C.; Kurrle, N.; Serve, H.; Gunther, U. L.; Schwalbe, H. *Angew. Chem., Int. Ed.* **2020**, *59* (6), 2304−2308.
(22) Wen, H.; An, Y. F.; Xu, W. J.; Kang, K. W.; Park, S. *Angew. Chem., Int. Ed.* **2015**, *54* (18), 5374−5377.
(23) Carvalho, J.; Alves, S.; Castro, M.; Geraldes, C.; Queiroz, J. A.; Fonseca, C. P.; Cruz, C. *J. Pharmacol. Toxicol. Methods* **2019**, *95*, 70−78.
(24) Hertig, D.; Maddah, S.; Memedovski, R.; Kurth, S.; Moreno, A.; Pennestri, M.; Felser, A.; Nuoffer, J. M.; Vermathen, P. *Analyst* **2021**, *146* (13), 4326−4339.
(25) Luchinat, E.; Cremonini, M.; Banci, L. *Chem. Rev.* **2022**, *122* (10), 9267−9306.
(26) Luchinat, E.; Barbieri, L.; Davis, B.; Brough, P. A.; Pennestri, M.; Banci, L. *J. Med. Chem.* **2024**, *67* (2), 1115−1126.
(27) Rydzik, A. M.; Brem, J.; van Berkel, S. S.; Pfeffer, I.; Makena, A.; Claridge, T. D.; Schofield, C. J. *Angew. Chem., Int. Ed.* **2014**, *53* (12), 3129−3133.
(28) Cheng, K.; Wu, Q.; Yao, C.; Chai, Z.; Jiang, L.; Liu, M.; Li, C. *JACS Au* **2023**, *3* (3), 849−859.
(29) Reivich, M.; Kuhl, D.; Wolf, A.; Greenberg, J.; Phelps, M.; Ido, T.; Casella, V.; Fowler, J.; Hoffman, E.; Alavi, A.; et al. *Circ. Res.* **1979**, *44* (1), 127−137.
(30) Dias, A. H.; Hansen, A. K.; Munk, O. L.; Gormsen, L. C. *EJNMMI Res.* **2022**, *12* (1), 15.
(31) Almuhaideb, A.; Papathanasiou, N.; Bomanji, J. *Ann. Saudi Med.* **2011**, *31* (1), 3−13.
(32) Tran-Dinh, S.; Courtois, A.; Wietzerbin, J.; Bouet, F.; Herve, M. *Biochimie* **1995**, *77* (4), 233−239.
(33) Shishmarev, D.; Fontenelle, C. Q.; Kuprov, I.; Linclau, B.; Kuchel, P. W. *Biophys. J.* **2018**, *115* (10), 1906−1919.
(34) Southworth, R.; Parry, C. R.; Parkes, H. G.; Medina, R. A.; Garlick, P. B. *NMR Biomed.* **2003**, *16* (8), 494−502.
(35) Liu, B. A.; Liu, C. X.; Zhou, X.; Fan, X. Y.; Huang, T.; Zhan, J. H.; Zhu, Q. J.; Zeng, D. Y.; Gong, Z.; He, L. C.; et al. *Anal. Chem.* **2024**, *96* (7), 3034−3043.
(36) Barbieri, L.; Luchinat, E. *J. Vis. Exp.* **2021**, No. 169, No. e62323.
(37) Sołtyka-Krajewska, M.; Ziemniak, M.; Zawadzka-Kazimierczuk, A.; Skrzypczyk, P.; Siwiak-Niedbalska, E.; Jaśkiewicz, A.; Zieliński, R.; Fokt, I.; Skóra, S.; Koźmiński, W.; et al. *Biomedicines* **2024**, *12* (10), 2240.
(38) Goldsmith, S. J.; Kostakoglu, L. A.; Somrov, S.; Palestro, C. J. *Radiol. Clin. N. Am.* **2005**, *43* (3), 571.
(39) Kanazawa, Y.; Umayahara, K.; Shimmura, T.; Yamashita, T. *NMR Biomed.* **1997**, *10* (1), 35−41.
(40) Li, A.; Luo, X.; Chen, D.; Li, L.; Lin, H.; Gao, J. *Anal. Chem.* **2023**, *95* (1), 70−82.
(41) Zhang, J.; Mitsis, E. M.; Chu, K.; Newmark, R. E.; Hazlett, E. A.; Buchsbaum, M. S. *J. Neurotrauma* **2010**, *27* (1), 35−49. Accessed Sep 25, 2024.
(42) Farhadi, P.; Yarani, R.; Valipour, E.; Kiani, S.; Hoseinkhani, Z.; Mansouri, K. *Biomed. Pharmacother.* **2022**, *146*, No. 112526.
(43) Zhang, Y.; Li, Q.; Huang, Z.; Li, B.; Nice, E. C.; Huang, C.; Wei, L.; Zou, B. *Cancers (Basel)* **2022**, *14* (19), 4568.
(44) Kanazawa, Y.; Yamane, H.; Shinohara, S.; Kuribayashi, S.; Momozono, Y.; Yamato, Y.; Kojima, M.; Masuda, K. *J. Neurochem* **1996**, *66* (5), 2113−2120.
(45) Coman, D.; Sanganahalli, B. G.; Cheng, D.; McCarthy, T.; Rothman, D. L.; Hyder, F. *Magn. Reson. Imaging* **2014**, *32* (4), 305−313.
(46) Siebeneicher, H.; Cleve, A.; Rehwinkel, H.; Neuhaus, R.; Heisler, I.; Müller, T.; Bauser, M.; Buchmann, B. *ChemMedChem* **2016**, *11* (20), 2261−2271.
(47) Zhu, Z.; Jiang, W.; McGinley, J. N.; Thompson, H. J. *Cancer Res.* **2005**, *65* (15), 7023−7030.
(48) Shin, Y. W.; Bae, E. A.; Cai, X. F.; Lee, J. J.; Kim, D. H. *Biol. Pharm. Bull.* **2007**, *30* (1), 197−199.
(49) Yarosh, D. B.; Galvin, J. W.; Nay, S. L.; Pena, A. V.; Canning, M. T.; Brown, D. A. *J. Dermatol. Sci.* **2006**, *42* (1), 13−21.
(50) Matsuda, H.; Wu, J. X.; Tanaka, T.; Iinuma, M.; Kubo, M. *Biol. Pharm. Bull.* **1997**, *20* (3), 243−248.
(51) Wang, D.; Ge, S.; Chen, Z.; Song, Y. *J. BUON* **2019**, *24* (5), 1824−1829.
(52) Yang, W.; Ma, L.; Li, S.; Cui, K.; Lei, L.; Ye, Z. *Molecules* **2017**, *22* (6), 943.
(53) Hung, Y.-C.; Pan, T.-L.; Hu, W.-L. *Oxid. Med. Cell Longev.* **2016**, *2016*, No. 5293284.
(54) Qi, H.; Chen, Z.; Qin, Y.; Wang, X.; Zhang, Z.; Li, Y. *Oncol. Lett.* **2022**, *23* (6), 184.
(55) Liu, Z. G.; Zhu, W. H.; Kong, X. Y.; Chen, X.; Sun, X. Y.; Zhang, W.; Zhang, R. W. *Oncol. Rep.* **2019**, *42* (5), 1893−1903.
(56) Charron, M. *Paediat. Respir. Rev.* **2006**, *7*, S41−S43.

https://doi.org/10.1021/acs.analchem.4c06149
Anal. Chem. 2025, 97, 9192−9201